EAST EUROPEAN JOURNAL OF PHYSICS. **3.** 19-31 (2022)
DOI:10.26565/2312-4334-2022-3-03 ISSN 2312-4334

7.379 % POWER CONVERSION EFFICIENCY OF A NUMERICALLY SIMULATED SOLID STATE DYE SENSITIZED SOLAR CELL WITH COPPER (I) THIOCYANATE AS A HOLE CONDUCTOR†

Eli Danladi[a,*], Muhammad Kashif[b], Thomas O. Daniel[c], Christopher U. Achem[d], Matthew Alpha[e], Michael Gyan[f]

[a]*Department of Physics, Federal University of Health Sciences, Otukpo, Benue State, Nigeria*
[b]*School of Electrical Automation and Information Engineering, Tianjin University, Tianjin 300072, China*
[c]*Department of Physics, Alex Ekwueme Federal University, Ndufu Alike, Ebonyi State, Nigeria*
[d]*Centre for Satellite Technology Development-NASRDA, Abuja, Nigeria*
[e]*Department of Physics, Nigerian Army University, Biu, Borno State, Nigeria*
[f]*Department of Physics, University of Education, Winneba, Ghana*
**Corresponding Author: Email: danladielibako@gmail.com, tel.: +2348063307256*
Received May 27, 2022; accepted June 20, 2022

Sourcing for alternative to liquid electrolyte in dye sensitized solar cells (DSSCs) have been the subject of interest in the photovoltaic horizon. Herein, we reported by means of simulation, the performance of dye sensitized solar cell by replacing liquid electrolyte with a copper (I) thiocyanate (CuSCN) hole conductor. The study was carried out using Solar Capacitance Simulation Software (SCAPS) which is based on poisson and continuity equations. The simulation was done based on a n-i-p proposed architecture of FTO/TiO_2/N719/CuSCN/Pt. Result of the initial device gave a Power Conversion Efficiency (PCE), Fill Factor (FF), Short Circuit Current Density (Jsc) and Open Circuit Voltage (Voc) of 5.71 %, 78.32 %, 6.23 mAcm^{-2}, and 1.17 V. After optimizing input parameters to obtain 1×10^9 cm^{-2} for CuSCN/N719 interface defect density, 280 K for temperature, 1.0 µm for N719 dye thickness, 0.4 µm for TiO_2 thickness, Pt for metal back contact, and 0.2 µm for CuSCN thickness, the overall device performance of 7.379 % for PCE, 77.983 % for FF, 7.185 mAcm^{-2} for Jsc and 1.317 V for Voc were obtained. When compared with the initial device, the optimized results showed an enhanced performance of ~ 1.29 times, 1.15 times, and 1.13 times in PCE, Jsc and Voc over the initial device. The results obtained are encouraging and the findings will serve as baseline to researchers involved in the fabrication of novel high-performance solid state DSSCs to realize its appealing nature for industry scalability.
Keywords: ssDSSC, Copper thiocyanate, Hole Conductor, SCAPs
PACS: 41.20.Cv; 61.43.Bn; *68.55.ag*; *68.55.jd*; 73.25.+i; 72.80.Tm; 74.62.Dh; 78.20.Bh; 89.30.Cc

INTRODUCTION

Issues linked to energy have drawn much research interest due to environmental impact and use of resources that cannot be replenished. Between 80 to 85 % of the global energy used today, comes from fossil fuels which its exploitation results to emission of dangerous pollutants such as nitrous oxide, hydrofluorocarbon, sulfur hexafluoride, carbon dioxide and volatile organic compounds, which has capacity to jeopardize future ecosystem. Photovoltaic has been seen as a promising renewable energy technology that has the ability of converting energy from the sun into electricity with enormous strength to solving problem connected to energy. Since after the report of O'Regan and Grätzel on efficient DSSC [1] based on nanostructured TiO_2 and iodide/tri-iodide (I^-/I^{3-}) redox specie, it has continued to gained attention of global researchers as a potential alternative to widely known silicon solar cell technology. This class of solar cell belongs to the third generation of photovoltaics and has the advantages of simpler production techniques, used of eco-friendly materials and cost effectiveness as compared with its counterpart [2,3].

The DSSC is made up of self-assembled mono-layer of dye in between the wide band gap, otherwise called the electron transport layer and the liquid mediator called the electrolyte [4,5]. However, liquid electrolyte is violent to the surrounding environment it operates which results to corrosive, photo-reactive, and highly volatile nature that affects the sealing status of the DSSCs and consequently, the effect of short-term performance and poor durability of the device is noticed [6]. Sourcing alternative to this liquid electrolyte have been the subject of interest in the photovoltaic horizon [7-9]. The solution to the aforementioned challenges is to replace the liquid electrolyte with solid state p-type semiconductor, this will take care of the leakage, heavy weight and architectural complexity.

The structure of a solid-state dye sensitized solar cell is depicted in Figure 1 [10], which shows its working principle. The dye absorbs photon energy, and then promote electron to the conduction band of the dye, and subsequently the electrons are transferred to the conduction band of the TiO_2. The dye that has lost electron regenerates through the process of hole injection from hole transport material. The electrons promoted to the TiO_2 conduction band flow through the network and are collected at the FTO and the holes within the hole transport material are collected at the counter electrode.

† ***Cite as***: E. Danladi, M. Kashif, T.O. Daniel, C.U. Achem, M. Alpha, and M. Gyan, East Eur. J. Phys. **3**, 19 (2022), https://doi.org/10.26565/2312-4334-2022-3-03

The solid-state semiconductor which are used in solid state dye solar cells and serves as replacement of liquid electrolytes evolved into three categories: organic, inorganic and carbonaceous. The three categories should have three main features which include: (1) their highest unoccupied molecular orbital and lowest unoccupied molecular orbital levels should be patterned in such a way as to match the highest occupied molecular orbital level of the dye and the conduction band of the TiO_2 to enhance the ability of charge transport [11], (2) the nature of the HTM must be amorphous, this is because TiO_2 pores filling is difficult with crystalline HTMs [11,12], (3) the mobility of the holes in the hole conductor should be high [13]. A quite number of p-type semiconductors have shown good ability to act as hole transport material in solar cell devices, which include, silicon carbide (SiC), copper iodide (CuI), Nickel oxide (NiO), copper thiocyanate (CuSCN), gallium nitride (GaN), 2,2′-7,7′-tetrakis (N,N-di-p-methoxyphenyl-amine) 9,9′-spirobifluorene (spiro-OMeTAD), poly(3,4-ethylenedioxythiophene):polystyrene sulfonate (PEDOT: PSS) to mention but a few [10,11,14,15].

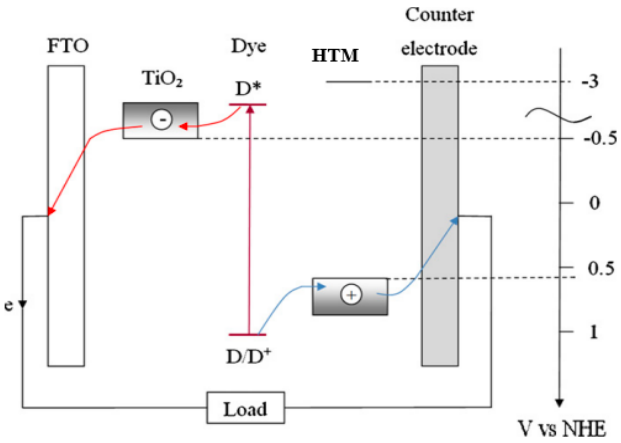

Figure 1. Schematic of a solid-state dye sensitized solar cell [10]

However, among the listed of them all, CuSCN has shown good prospect due to its display of extraordinary stability as a result of polymeric nature properties from the solid [15,16]. It was demonstrated by Perera and Tennakone [17], that it is often difficult for CuSCN to decompose into SCN^{-1}, and by means of stoichiometric, SCN^{-1} does not result to surface trapping in CuSCN, which makes devices developed with CuSCN has minimal recombination and high stability [18].

In this paper, a simulation studies on dye sensitized solar cell was carried out by replacing liquid electrolyte with CuSCN inorganic salt as HTM. The results demonstrate that, CuSCN is an alternative to liquid based electrolyte and this is projected to serve as a baseline for researchers involved in fabrication and design of high efficient dye-based solar cells with durable properties.

SIMULATION USING SCAPS

We employed the use of Solar Cell Capacitance Simulator Software in one Dimension (SCAPS-1D) to model and simulate the solid state dye sensitized solar cells. The software basically works on two basic semiconductor equations, which include, the poisson equation and the continuity equation of electrons and holes under steady-state condition [19]. The SCAPS-1D was used under the air mass (AM 1.5G) at 100 mWm^{-2} and temperature of 300 K to obtain the current-voltage (J–V) photovoltaic characteristics of ssDSSCs. The planar heterojunction n-i-p cell structure was employed in the study with architecture of FTO/TiO_2/N719/CuSCN/Pt as shown in Figure 2. The data used for the simulation were obtained from literatures and listed in Table 1 with sources duly acknowledged. The front and back contacts are fluorine tine oxide and platinium with work functions of 4.4 eV and 5.65 eV. The defect interface for the CuSCN/N719 are as shown in Table 2.

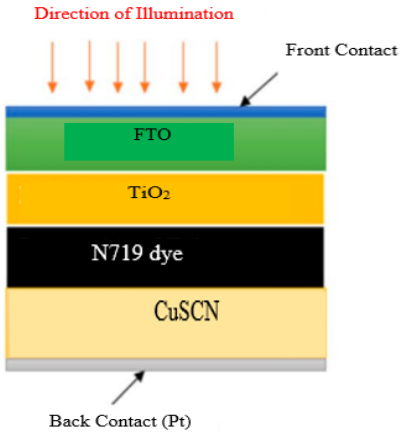

Figure 2. Device structure of the n–i–p solid state dye sensitized solar cell.

Table 1. Parameters used for simulation of perovskite solar cell structures using SCAPS-1D [11,18,20],

Parameters	FTO	TiO_2	N719	CuSCN
Thickness (μm)	0.4	0.05	0.6	0.2
Band gap energy Eg (eV)	3.5	3.2	2.33	3.6
Electron affinity χ (eV)	4.0	4.2	3.9	1.7
Relative permittivity ϵ_r	9.0	10	30	10
Effective conduction band density Nc (cm^{-3})	2.2×10^{18}	2.2×10^{18}	2.4×10^{20}	1×10^{21}
Effective valance band density Nv (cm^{-3})	2.2×10^{18}	2.2×10^{18}	2.5×10^{20}	1×10^{21}
Electron mobility μn ($cm^2\ V^{-1}\ s^{-1}$)	20	20	5.0	100
Hole mobility μp ($cm^2\ V^{-1}\ s^{-1}$)	10	10	5.0	25
Donor concentration N_D (cm^{-3})	1×10^{19}	1×10^{17}	0	0
Acceptor concentration N_A (cm^{-3})	0	0	1×10^{17}	1×10^{17}
Defect density Nt (cm^{-3})	1×10^{15}	1×10^{13}	1×10^{15}	1×10^{22}

Table 2. Parameters of interface layer [11,18]

Parameters	CuSCN/N719 dye
Defect type	Neutral
Capture cross section for electrons (cm^2)	1×10^{-19}
Capture cross section for holes (cm^2)	1×10^{-19}
Energetic distribution	Single
Energy level with respect to Ev (eV)	0.1
Characteristic energy (eV)	0.650
Total density (cm^{-3})	1×10^{12}

RESULTS AND DISCUSSIONS

Current-voltage and Quantum Efficiency Characteristics of initial device

The current voltage plot demonstrates the characteristic pattern that is often used for determination of photovoltaic performance parameters of the power output of a solar device. The J-V plot of our simulated device under light illumination is as shown in Figure 3(a).

The studies under standard photovoltaic performance results to Jsc of 6.23 $mAcm^{-2}$, Voc of 1.17 V, FF of 78.32 and PCE of 5.71 %. As shown in Figure 3(b), the J-V characteristics without illumination is a diodic behavior, where no current is flowing and demonstrates a rectifying characteristics.

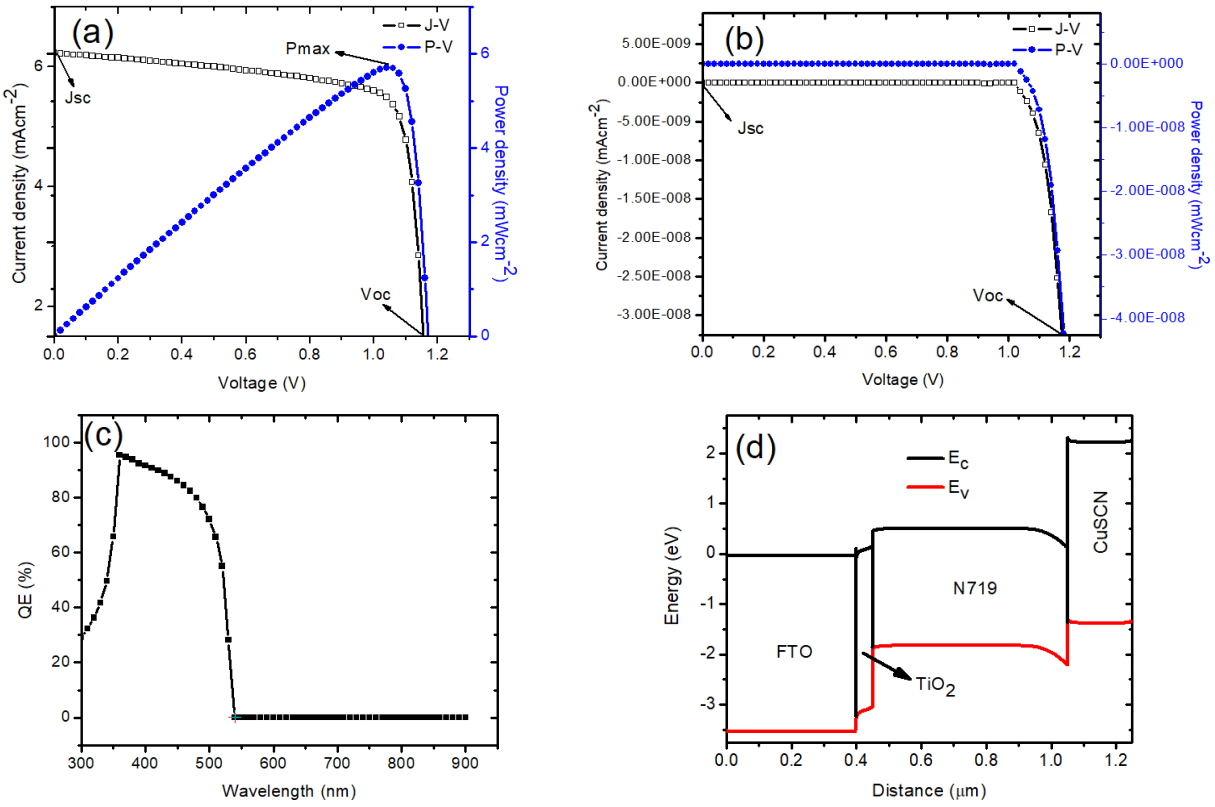

Figure 3. (a) J-V & P-V curve of initial device under illumination, (b) J-V & P-V curve of initial device in the dark, (c) QE curve of the device with respect to wavelength and (d) Energy band diagram of the device

The Voc of the ssDSSC device is the voltage through which current flows in the circuit when the polarities of the device are not in touch. This is the favourable voltage generated by the ssDSSC device. The dependency relationship that exist between Voc, Jsc is shown in equation 1. The Jsc here is the current generated by the ssDSSC device under illumination when the device is short-circuited. The FF is the ratio between product of maximum current and voltage to the product of Voc and Jsc of the ssDSSCs as shown in equation 2. The quality of the simulated ssDSSC is described in terms of this parameter [20]. The PCE of the ssDSSC is obtained as the ratio of maximum power (P_{max}) and incident power (P_{in}) as expressed in equation 3.

$$V_{oc} = \frac{nK_BT}{q} \ln\left[\frac{J_{sc}}{J_o} + 1\right] \tag{1}$$

$$FF = \frac{P_{\max}}{J_{sc} \times V_{oc}} = \frac{J_{mp} \times V_{mp}}{J_{sc} \times V_{oc}} \tag{2}$$

$$PCE = \frac{P_{\max}}{P_{in}} = \frac{V_{oc} \times J_{sc} \times FF}{P_{in}} \times 100\% \tag{3}$$

When we compare our simulated result with obtained experimental result reported by Premalal et. al [21], using same ETM, HTM and dye, there was improved performance in our result of ~ 1.81, ~ 1.88 and ~ 1.35 times in Voc, FF and PCE (see Table 3). Their ssDSSC device gave a record value of PCE=4.24 %, Jsc=15.76, Voc=0.647 and FF=41.60 %. The differences are due to low conductivity in CuSCN as a result of carbon paste as metal back contact as against the Pt back contact reported in our study. There was also an overlap behaviour of hole diffusion in the bulk CuSCN and charge transfer at the CuSCN/carbon interface which result to recombination at the TiO_2/CuSCN interface. At the CuSCN/Pt, charge transfer resistance is lowered and reactive surface area is extended [21]. Further comparison with ssDSSC simulated with ZnO as ETM, N719 as dye, CuSCN as HTM and Au as metal back contact gave photovoltaic parameters close to those reported in our studies [18] as shown in Table 3.

Table 3. Photovoltaic parameters obtained from simulation compared to experimental data

Parameters	Experimental [21]	Simulated [18]	Present Study
Jsc	15.760	8.563	6.23
Voc	0.647	0.885	1.17
FF	41.600	70.940	78.32
PCE	4.240	5.380	5.71

Quantum efficiency (QE) is one of the crucial characteristic of solar cell which is the ratio of the electron–hole pairs collected to the number of striking photons [11,22]. QE is seen as a function of wavelength in nm or photon energy in eV. Equation 4 expresses the relationship between QE and current density.

$$J_{sc} = q\int \varphi(\lambda) QE(\lambda) d\lambda \tag{4}$$

Where, $\phi(\lambda)$ is the energy intensity per wavelength (λ) bandwidth unit. Figure 3(c), shows the quantum efficiency versus wavelength for the simulated ssDSSC device, which explains how photon energy is transformed into electricity as a function of wavelengths [23]. The curve was within the wavelength range of 300-900 nm. The QE of the ssDSSC increased from 30.42 % at 300 nm to a maximum of 96.2 % at 356 nm but gradually decreases to 0.16 % at a wavelength value of 540 nm. As seen from our study, it is worthy of note to know that energy losses as a result of exiton quenching is experienced beyond 540 nm. The device can absorb sufficient photon energy within visible region to be converted to electricity, however at longer wavelength, the QE decreases gradually. Consequently, at ~ 540 nm, ssDSSC device becomes weakly efficient to absorb photon energy due to limited ability to harvest photon energy at extended wavelength due to high rate of carrier recombination [18]. Figure 3(d) shows the energy band structure of the device. The interface conduction and valence band offset at the TiO_2/N719 and N719/CuSCN interfaces are ΔEc=0.33 eV, ΔEv=1.22 eV and ΔEc=2.08 eV, ΔEv=0.81 eV. The value of ΔEc at the TiO_2/N719 interface prevents the flow of electrons from the TiO_2 layer to N719 dye to avoid recombination. While the value of ΔEv at the N719/CuSCN interface denies the flow of holes to the metal-back contact to prevent their recombination at the CuSCN layer. These values obtained are crucial in determining high PCE by encouraging sufficient collection of charge carriers.

Effect of CuSCN/N719 defect

The interface defect density between the hole conductor CuSCN and the absorbing dye was varied from 10^9 cm^{-2} to 10^{13} cm^{-2} while keeping other parameters constant during the simulation. The PCE, Jsc and Voc were significantly affected by increase in interface density. The PCE, Jsc and Voc decrease from 6.94 to 5.70 %, 6.87 to 6.22 $mAcm^{-2}$ and 1.31 to 1.17 V (see Table 4). Surprisingly, Voc remains constant above 10^{12} cm^{-2}. Once such a threshold is attained,

further increase in interface defect density does not affect the Voc because carrier generation occurs very close to that point and shows maximum carrier saturation. This is in agreement with previous report by Devi et al. [24], that is linked to high trapping sites and results to possible recombination with increase in defect density and also in accordance with reported literatures [18,25]. We can speculate from our result that, interface defect density has an inverse relationship with PV performance, which means that, increasing defect in the CuSCN/dye interface of ssDSSC results to reduction in diffusion length [18]. Figure 4(a), (b) and (c), show the relationship that exist between current and voltage, QE and wavelength and between power density and open circuit voltage. The QE rises steadily from 29.5 % at 300 nm to 99, 98, 97, 95 and 94 % with increase in interface defect density at 360 nm before it fell back with QE of 0.44 % at 540 nm. This exhibits good agreement in conformity to similar studies by Korir et al. [18]. Figure 4(c) expresses the maximum power ranging from 5.70 to 6.94 $mWcm^{-2}$.

Table 4. Photovoltaic parameters with varied CuSCN/dye defect interface

Interface defect	PCE	FF	Jsc	Voc
1×10^{9}	6.94	77.03	6.87	1.31
1×10^{10}	6.26	77.64	6.56	1.23
1×10^{11}	5.80	78.08	6.29	1.18
1×10^{12}	5.71	78.32	6.23	1.17
1×10^{13}	5.70	78.36	6.22	1.17

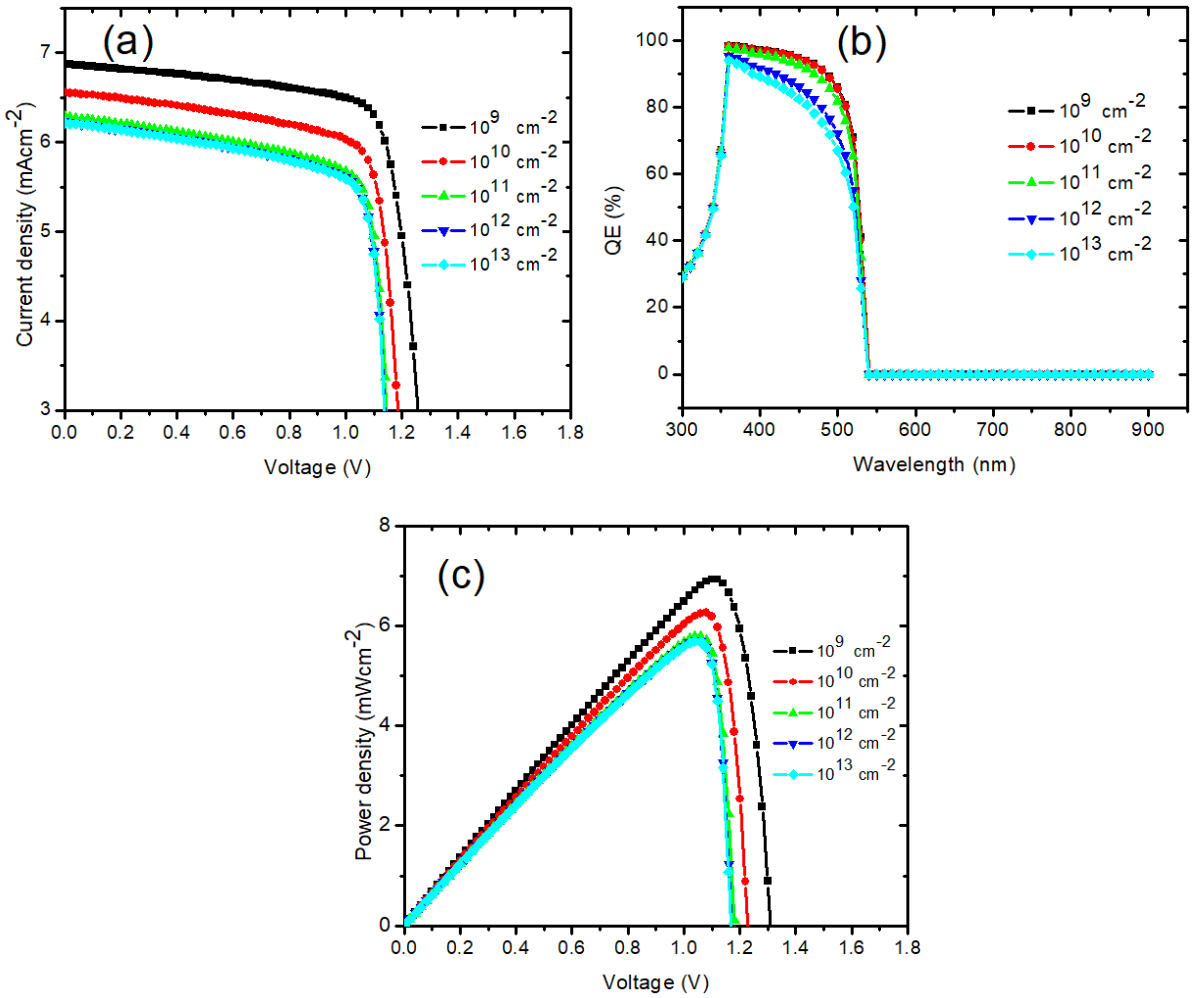

Figure 4. (a) J-V plots with varied CuSCN/dye defect density, (b) QE versus wavelength with varied CuSCN/dye defect density and (c) P-V plots with varied CuSCN/dye defect density

Effect of Temperature

The temperature with which a given solar cell operates is crucial in determining the device output performance [11,18]. The working temperature of the simulated ssDSSC device was varied from 270 K to 340 K with all other parameters constant. As depicted in Table 5, the photovoiltaic performance of ssDSSC is affected by the temperature. Increasing the temperature from 270 K to 340 K results to dramatic decrease in PCE and Voc. Similar trend was reported by other researchers [11,18,26-29]. This could be attributed to the fact that, at higher temperature, the electrons in the

device absorbs sufficient energy and quickly becomes unstable and subsequently result to recombination before they reach the depletion region and thereby prompt the reduced solar PCE [11,27]. The decrease in PV parameters with increasing temperature can be further explained thus: the band gap of semiconducting materials decreases when temperature is high and Voc has a direct relationship with bandgap, so Voc decreases with increasing temperature, as such, the efficiency also decreases simultaneously with increase in temperature [28,29]. Surprisingly, the fill factor and Jsc were increased with temperature increase which demonstrates an inverse relationship between the parameters. The Jsc gradually increase from 6.218 to 6.232 mAcm^{-2}, which is attributed to improved generation of charge carriers and reduced bandgap which results to exitonic quenching of carriers at the heterojunction barrier when the thermal activation energy increases [18,30,31]. Figure 5(a) shows the J-V characteristic curve with different temperature. The correlation between PCE and FF and between Jsc and Voc is depicted in Figures 5(b) and (c). Table 5 summarized the photovoltaic performance with varied temperature.

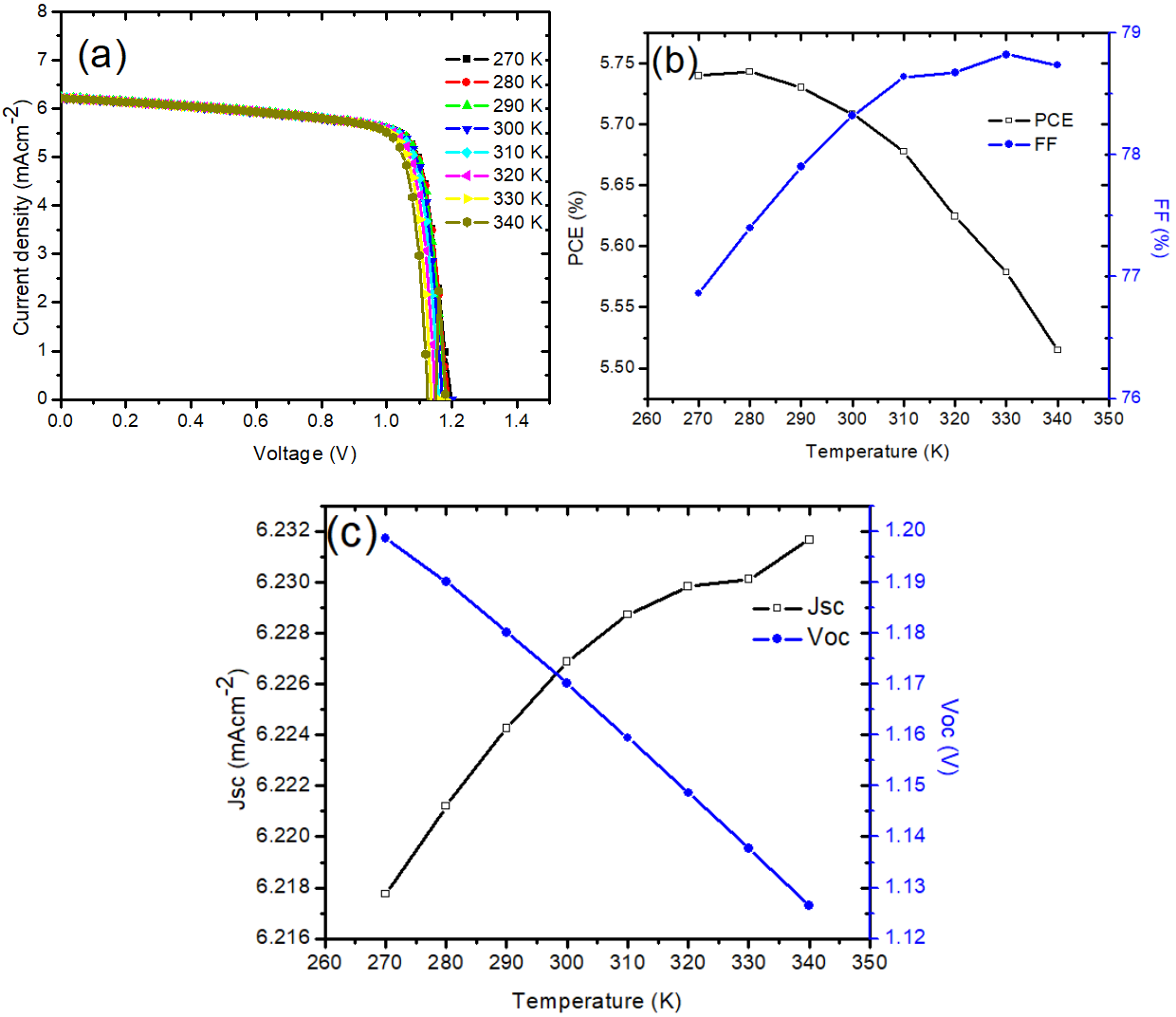

Figure 5. (a) J-V curve with varied temperature, (b) PCE and FF correlation with temperature and (c) Jsc and Voc correlation with temperature

Table 5. Photovoltaic parameters with varied temperature

Tempt (K)	PCE	FF	Jsc	Voc
270	5.74	76.86	6.218	1.20
280	5.74	77.40	6.221	1.19
290	5.73	77.90	6.224	1.18
300	5.71	78.32	6.227	1.17
310	5.68	78.64	6.229	1.16
320	5.62	78.67	6.230	1.15
330	5.58	78.82	6.231	1.14
340	5.51	78.74	6.232	1.13

Effect of dye thickness

Photosensitizer is a crucial material in determining the metrics of ssDSSC. The dye used in this simulation study is a N719 dye. The dye thickness was varied from 0.2 µm to 1.0 µm (see Figure 6(a)).

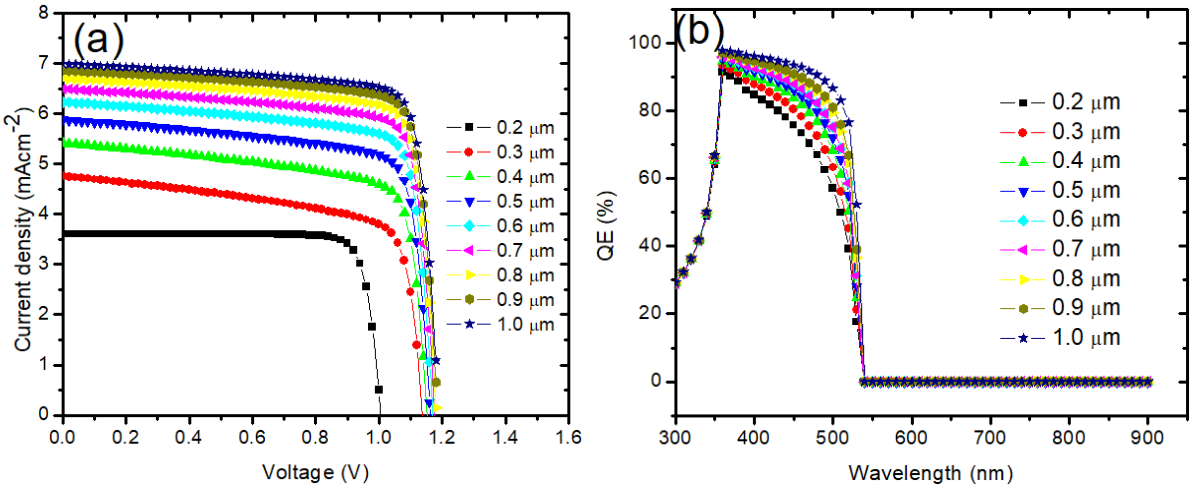

Figure 6. (a) J-V curve with varied N719 dye thickness, (b) QE versus wavelength with varied N719 dye thickness

The N719 dye molecule harvest the energy from the sun and convert it into electrical energy at the junction [18,31]. For the dye to meet its requirements in ssDSSC, it should be able to harvest light at the visible and near infra-red region of electromagnetic spectrum [18,32,33]. The thickness of dye pigment has significant effect on metric parameters (PCE, FF, Jsc and Voc) of the solar cell device. Table 6 shows the dependency of PCE, FF, Jsc and Voc with N719 dye thickness.

Table 6. Photovoltaic parameters with varied N719 dye thickness

Thickness	PCE	FF	Jsc	Voc
0.2	3.076	68.367	3.601	1.117
0.3	3.805	71.285	4.757	1.138
0.4	4.634	74.361	5.407	1.153
0.5	5.252	76.835	5.879	1.163
0.6	5.710	78.319	6.230	1.170
0.7	6.062	79.372	6.493	1.176
0.8	6.344	80.180	6.697	1.181
0.9	6.566	80.716	6.858	1.186
1.0	6.743	81.082	6.987	1.190

All photovoltaic parameters increased drastically with increase in thickness of the N719 dye. The PCE was increased from 3.076 % to 6.743 %, the FF improved from 68.367 to 81.082 %, Jsc increased from 3.601 $mAcm^{-2}$ to 6.987 $mAcm^{-2}$ and Voc increased from 1.117 V to 1.190 V. The increase observed in the parameters was as a result of generation of many electron-hole (e-h) pairs due to sufficient dye adsorption on the surface of the TiO_2 nano material that promote electron into conduction band of the semiconductor linked to the device [18,33]. When the thickness is low, there is incomplete absorption of photons due to poor adsorption on the semiconductor surface, as a result, some of the unabsorbed surface act as recombination centres leading to electron transport resistance which consequently leads to poor device performance. Figure 6(b) shows the relationship between QE and wavelength. The QE increases gradually from 28.90 % at 300 to 97.93 % at 356 nm and starts decreasing to 1.03 % at 540 nm. The sweeping is within the visible region which is a satisfied condition for light harvesting material in our simulation. Figures 7(a-d), show the metric parameters dependence with thickness of the dye. The optimum performance was with device with 1.0 µm thickness, which demonstrates a PCE of 6.743 %, FF of 81.082 %, Jsc of 6.987 $mAcm^{-2}$ and Voc of 1.190 V.

Effect of TiO_2 thickness

Several researchers have reported the influence of TiO_2 thickness on the performance of solar cells [11,34,35]. To show the influence of the TiO_2 thickness on PV parameters, we varied the thickness from 0.1 µm to 0.8 µm. Figure 8 shows the J-V curve of the simulation with different thickness. Figures 9(a-d) show the correlation between the performance parameters and the TiO_2 thickness. As shown in Table 7, the PCE increased from 5.705 to 5.743 % at thickness of 0.1 µm to 0.4 µm. Beyond 0.4 µm, the device performance degrades which can be explained thus: the thicker the TiO_2, the higher the surface adsorption between the dye and the semiconductor and the more its photon absorption capability. Literature has reported a direct proportionality existing between dye adsorption of TiO_2 and the TiO_2 thickness

(i.e. the more the thickness of TiO_2, the more the bonding formation it has with dye) [36]. The optimized thickness is 0.4 µm which gave a PCE value of 5.743 %. The Jsc was also higher at the same thickness. The improved Jsc (6.121 $mAcm^{-2}$) was due to enhanced dye anchorage with the thicker TiO_2. Beyond the 0.4 µm thickness of TiO_2, the PCE and Jsc decreases, which is attributed to lower transmittance that limit solar radiance on the dye and it is in agreement with previously reported document [37].

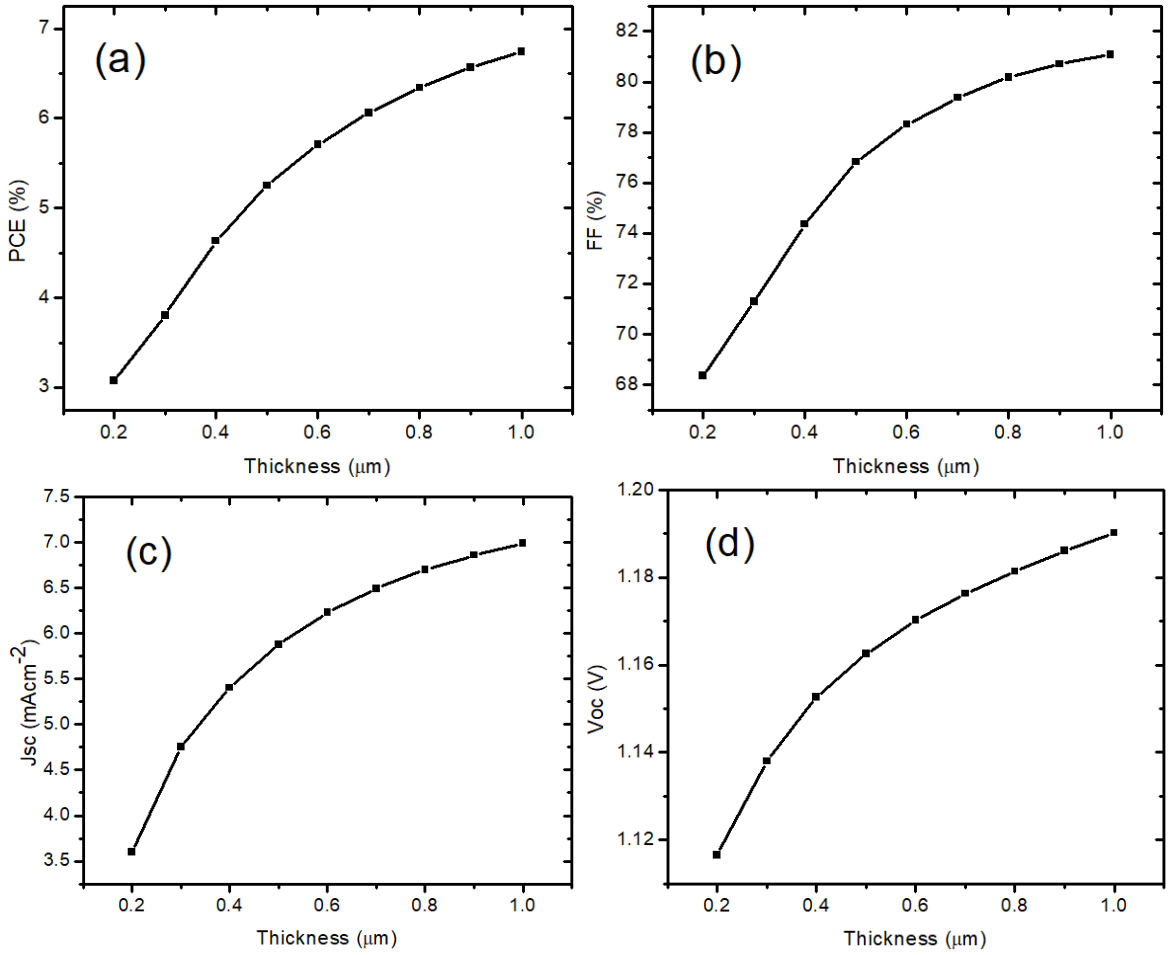

Figure 7. variation of (a) PCE, (b) FF, (c) Jsc and (d) Voc with thickness of N719 dye

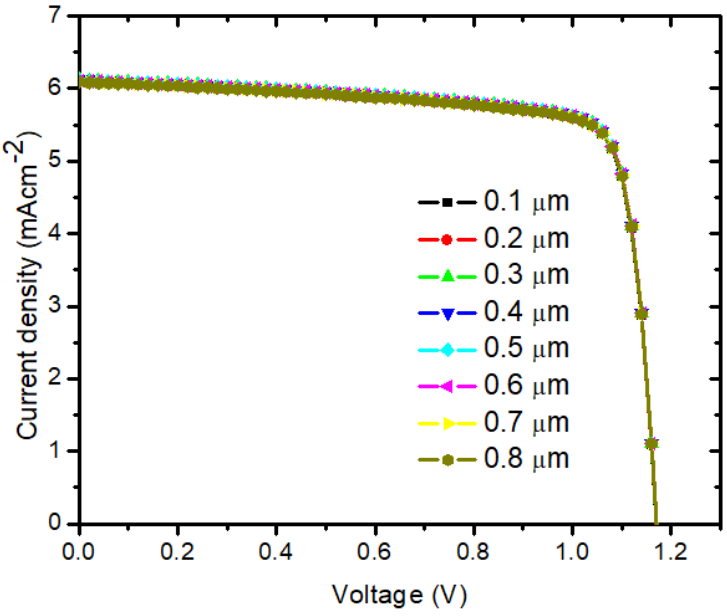

Figure 8. J-V curves with variation of thickness of TiO_2

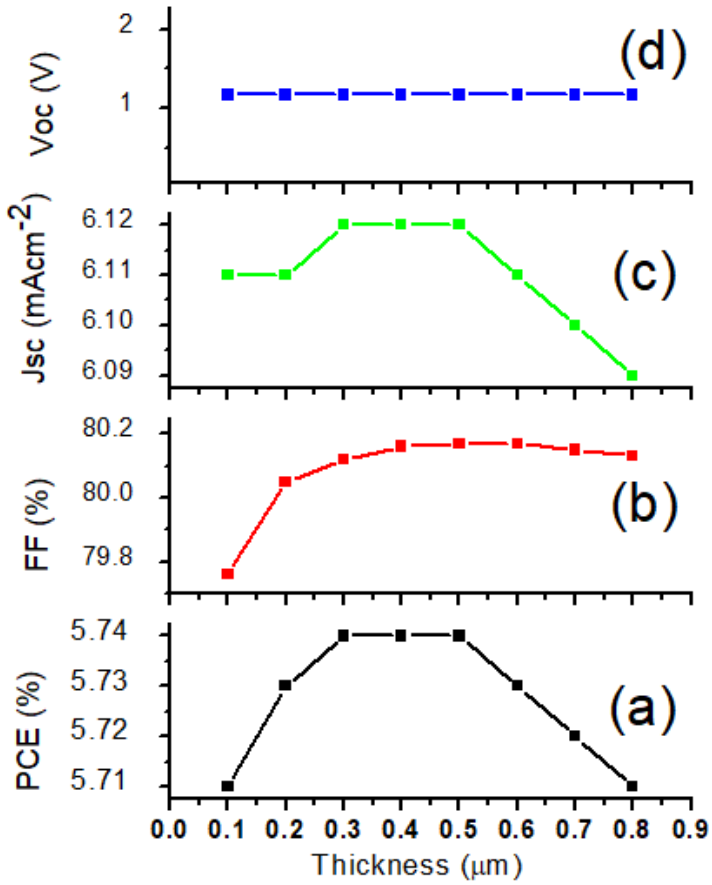

Figure 9. variation of (a) PCE, (b) FF, (c) Jsc and (d) Voc with thickness of TiO_2

Table 7. Photovoltaic parameters with varied TiO_2 thickness

Thickness	PCE	FF	Jsc	Voc
0.1	5.7054	79.7597	6.112232	1.170321
0.2	5.7273	80.0494	6.112714	1.170455
0.3	5.7392	80.1239	6.119313	1.170540
0.4	5.7433	80.1602	6.120635	1.170592
0.5	5.7412	80.1719	6.117325	1.170621
0.6	5.7340	80.1680	6.109958	1.170634
0.7	5.7228	80.1539	6.099061	1.170634
0.8	5.7082	80.1334	6.085118	1.170626

Effect of back contact

The photovoltaic parameters of ssDSSC is influenced by the type of metal contact used. Several metal back contacts have been reported in literatures [11,18, 30-38]. In our simulation, we made used of Ni, Au, Pd and Pt as the back contacts. Surprisingly, from our investigation, the metal back contact has no effect on the performance output of our device. This is because, by using CuSCN as hole conductor, the total internal resistances of the ssDSSCs remained unchanged as such there is no further carrier generation. The interfacial resistance at the CuSCN/metal back contact was unaffected which results to negligible ohmic contact. A report that shows negligible effect of metal contact on device was demonstrated by Behrouznejad et al. [38] where a HTM and HTM-free devices were developed. The impact was negligible in devices with HTM. Table 8 shows the comparison in the PV parameters.

Table 8. Photovoltaic parameters with different metal back contact

Parameter	PCE	FF	Jsc	Voc
Ni	5.71	78.32	6.23	1.17
Au	5.71	78.32	6.23	1.17
Pd	5.71	78.32	6.23	1.17
Pt	5.71	78.32	6.23	1.17

Figures 10(a) and (b) show the J-V and QE curves with different metal contact. Figure 11 shows the PV parameters with different back metal contact.

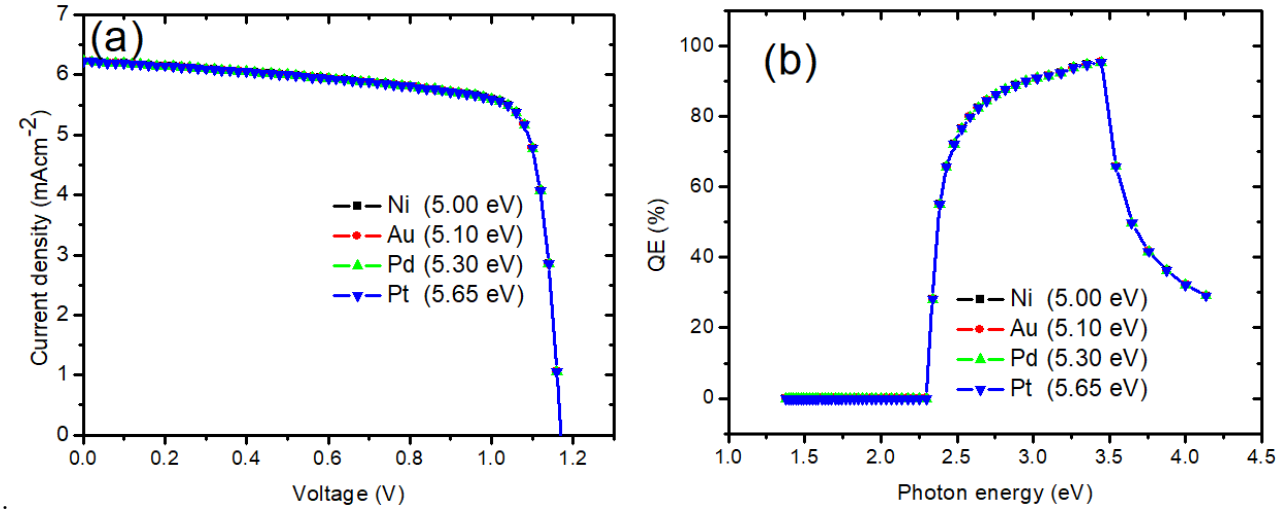

Figure 10. (a) J-V curves and (b) QE curves with different metal back contact

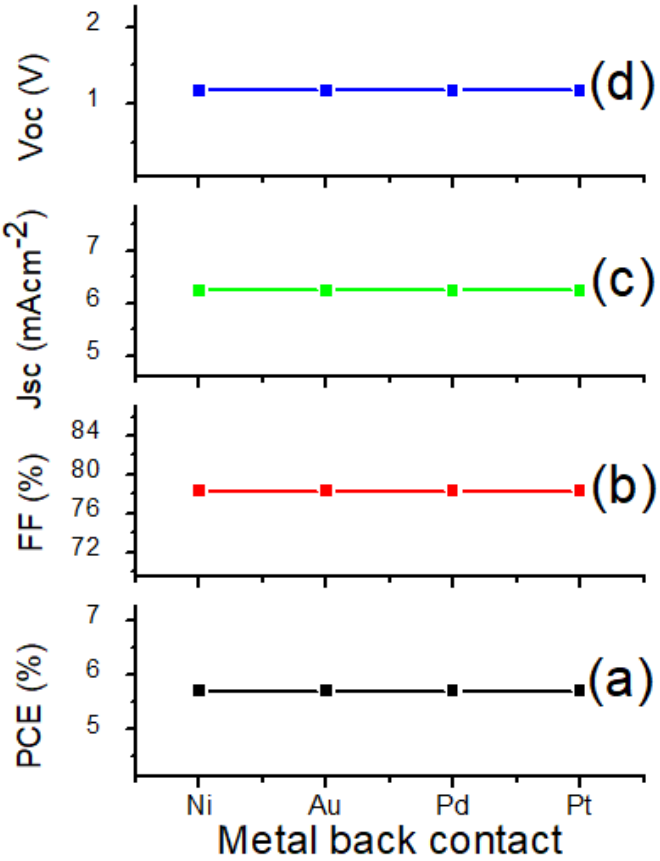

Figure 11. variation of (a) PCE, (b) FF, (c) Jsc and (d) Voc with different metal back contact

Effect of CuSCN thickness

The HTM is an important part of ssDSSCs which play a significant role in determining the performance of the overall device through photo-thermal stabilities [18]. The thickness of CuSCN was varied from 0.1 µm to 0.8 µm (see Figure 12) and the parameters; FF, PCE, Voc and Jsc were evaluated under standard photovoltaic conditions. The values of the parameters all remained unchanged throughout the simulation. The PCE = 5.71 %, FF = 78.32 %, Jsc =6.23 mAcm^{-2} and Voc = 1.17 V. The results obtained here show that, the CuSCN HTM is efficient at all thicknesses considered during the simulation and has the ability to effectively work in the proposed architecture in our simulation. Figures 13(a-d) show the relationship between the performance parameters and the CuSCN thickness.

Optimized device

The optimization was done by chosen the parameter that gave the optimum performance upon variation within a selected range. For the CuSCN/N719 interface defect density, an optimum value of 1×10^{9} cm^{-2} was obtained, while 280 K was optimum temperature, 1.0 µm was optimum thickness for N719 dye, 0.4 µm was optimum value for TiO_2 thickness, Pt was still used as the back contact since the back contact is not affected in our simulation, and 0.2 µm for CuSCN thickness. After putting the optimized values, an overall device performance of 7.379 % for PCE, 77.983 % for FF, 7.185 $mAcm^{-2}$ for Jsc and 1.317 V for Voc were obtained. The optimized results showed an improved performance of ~ 29.25 %, 15.36 %, and 12.56 % in PCE, Jsc and Voc over the initial device.

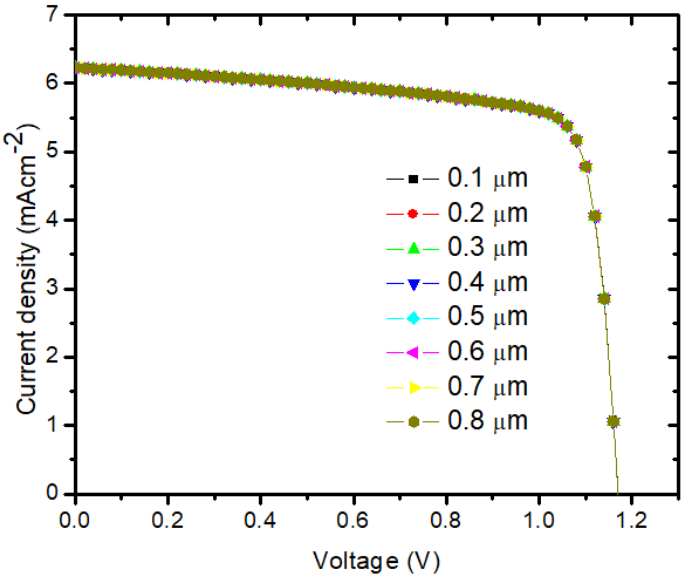

Figure 12. J-V curves with varied thickness of CuSCN

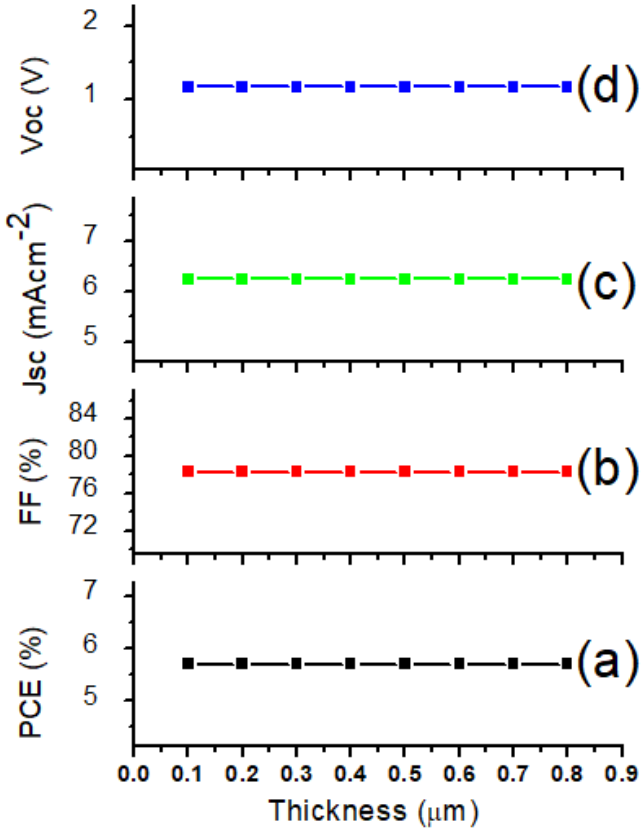

Figure 13. (a) PCE, (b) FF, (c) Jsc and (d) Voc with different CuSCN thickness

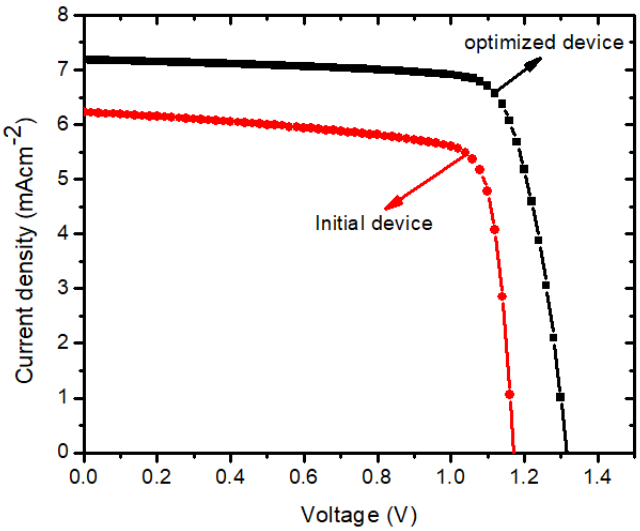

Figure 14. Combine J-V curves for the initial and optimized device

CONCLUSION

We reported the performance of a solid state dye sensitized solar cell based on CuSCN as a hole conductor using SCAPS-1D. The performance of the overall ssDSSC was achieved by optimizing the CuSCN/dye interface defect, operating temperature, CuSCN thickness, TiO_2 thickness and N719 dye thickness through data variation. The optimized device results to 7.379 % PCE, 77.983 % FF, 7.185 $mAcm^{-2}$ Jsc and 1.317 V Voc. This research suggests that, efficient stable and durable dye sensitized solar cells can be achieved by replacing liquid electrolyte with CuSCN hole conductor that is cost effective.

Acknowledgement

The authors would like to thank Professor Marc Burgelman, Department of Electronics and Information Systems, University of Gent for the development of the SCAPS software package and allowing its use.

Conflict of interest. Authors have declared that there was no conflict of interest.
Funding. This article did not receive any funding support.

ORCID IDs

Eli Danladi, https://orcid.org/0000-0001-5109-4690; **Thomas O. Daniel**, https://orcid.org/0000-0002-5176-9181

REFERENCES

[1] B. O'regan, and M. Grätzel, Nature, **353**, 737–740 (1991), https://doi.org/10.1038/353737a0
[2] S. Sharma, K.K. Jain, and A. Sharma, Materials Sciences and Applications, **6**(12), 1145–1155 (2015), https://doi.org/10.4236/msa.2015.612113
[3] V.R. Gómez, F.A. Mató, D.S. Jiménez, G.S. Rodríguez, A.Z. Lara, I.M. De Los Santos, and H.Y.S. Hernández, Optical and Quantum Electronics, **52**, 324 (2020), https://doi.org/10.1007/s11082-020-02437-y
[4] A. Hagfeldt, G. Boschloo, L.C. Sun, L. Kloo, and H. Pettersson, Chemical Reviews, **110**, 6595–6663 (2010), https://doi.org/10.1021/cr900356p
[5] M. Gratzel, Accounts of Chemical Research, **42**, 1788–1798 (2009), https://doi.org/10.1021/ar900141y
[6] S. Yanagida, Y.H. Yu, and K. Manseki, Accounts of Chemical Research, **42**, 1827–1838 (2009), https://doi.org/10.1021/ar900069p
[7] I. Chung, B. Lee, J. He, R.P.H. Chang, and M.G. Kanatzidis, Nature, **485**, 486-489 (2012), https://doi.org/10.1038/nature11067
[8] M. Wang, N. Chamberland, L. Breau, J.E Moser, R.H. Baker, B. Marsan, S.M. Zakeeruddin, and M. Grätzel, Nature Chemistry, **2**, 385–389 (2010), https://doi.org/10.1038/nchem.610
[9] A. Yella, H.W. Lee, H.N. Tsao, C. Yi, A.K. Chandiran, M.K. Nazeeruddin, E.W.G. Diau, C.Y. Yeh, S.M. Zakeeruddin, and M. Grätzel, Science, **334**, 629–634 (2011), https://doi.org/10.1126/science.1209688
[10] K.H. Wong, K. Ananthanarayanan, S.R. Gajjela, and P. Balaya, Materials Chemistry and Physics, **125,** 553-557 (2011), https://doi.org/10.1016/j.matchemphys.2010.10.017
[11] F. Jahantigh, and M.J. Safkhani, Applied Physics A, **125**, 276 (2019), https://doi.org/10.1007/s00339-019-2582-0
[12] L. Schmidt-Mende, S.M. Zakeeruddin, and M. Grätzel, Applied Physics Letters, **86**, 013504 (2005), https://doi.org/10.1063/1.1844032
[13] W. Zhang, Y. Cheng, X. Yin, and B. Liu, Macromolecular Chemistry and Physics, **212**, 15-23 (2011), https://doi.org/10.1002/macp.201000489
[14] F. Arith, O.V. Aliyaselvam, A.N.M. Mustafa, M.K. Nor, and O.A. Al-Ani, International journal of renewable energy research, **11**(2), 869-878 (2021), https://www.ijrer.org/ijrer/index.php/ijrer/article/view/12046/pdf
[15] E.V.A. Premalal, G.R.R.A. Kumara, R.M.G. Rajapakse, M. Shimomura, K. Murakami, and A. Konno, Chemical Communication, **46**, 3360–3362 (2010), https://doi.org/10.1039/B927336K

[16] R. Hehl, and G. Thiele, Anorganische und Allgemeine Chemie, **626**, 2167–2172 (2000), https://doi.org/10.1002/1521-3749(200010)626:10%3C2167::AID-ZAAC2167%3E3.0.CO;2-7
[17] V. Perera, and K. Tennakone, Solar Energy Materials and Solar Cells, **79**(2), 249–255 (2003), https://doi.org/10.1016/S0927-0248(03)00103-X
[18] B.K. Korir, J.K. Kibet, and S.M. Ngari, Optical and Quantum Electronics, **53**, 368 (2021), https://doi.org/10.1007/s11082-021-03013-8
[19] M. Burgelman, J. Verschraegen, S. Degrave, and P. Nollet, Progress in Photovoltaics: Research and Applications, **12**(2–3), 143-153 (2004), https://doi.org/10.1002/pip.524
[20] D. Bartesaghi, I. del Carmen Pérez, J. Kniepert, S. Roland, M. Turbiez, D. Neher, and L.J.A. Koster, Nature Communications, **6**(1), 1–10 (2015), https://doi.org/10.1038/ncomms8083
[21] E.V.A. Premalal, N. Dematage, and A. Konno, Chemistry Letters, **41**, 510-512 (2012), https://doi.org/10.1246/cl.2012.510
[22] A.M. Karmalawi, D.A. Rayan, and M.M. Rashad, Optik, **217**, 164931 (2020), https://doi.org/10.1016/j.ijleo.2020.164931
[23] A.J. McEvoy, L. Castaner, T. Markvart, in: *Solar cells: materials, manufacture and operation*, (Academic Press, Amsterdam. 2013), pp. 3–25.
[24] N. Devi, K.A. Parrey, A. Aziz, and S. Datta, Journal of Vacuum Science & Technology B: Microelectronics and Nanometer Structures Processing, Measurement, and Phenomena, **36**(4), 04G105 (2018), https://doi.org/10.1116/1.5026163
[25] Y. Gan, X. Bi, Y. Liu, B. Qin, Q. Li, Q. Jiang, and P. Mo, Energies, **13**(22), 5907 (2020), https://doi.org/10.3390/en13225907
[26] A.K. Daoudia, Y. El Hassouani, and A. Benami, International Journal of Engineering and Technical Research, **6**(2), 71-75 (2016), https://www.academia.edu/download/54231833/IJETR042544.pdf
[27] U. Mehmood, A. Al-Ahmed, F.A. Al-Sulaiman, M.I. Malik, F. Shehzad, and A.U.H. Khan, Renewable and Sustainable Energy Reviews, **79**, 946 (2017), https://doi.org/10.1016/j.rser.2017.05.114
[28] P. Roy, S. Tiwari, and A. Khare, Results in Optics, **4**, 100083 (2021), https://doi.org/10.1016/j.rio.2021.100083
[29] S. Dubey, J.N. Sarvaija, and B. Seshadri, Energy Procedia, **33**, 311-321 (2013), https://doi.org/10.1016/j.egypro.2013.05.072
[30] A. Shahriar, S. Hasnath, and M.A. Islam, EDU Journal of Computer and Electrical Engineering, **01**(01), 31-37 (2020), https://doi.org/10.46603/ejcee.v1i1.21
[31] C. Xiang, X. Zhao, L. Tan, J. Ye, S. Wu, S. Zhang, and L. Sun, Nano Energy, **55**, 269–276 (2019), https://doi.org/10.1016/j.nanoen.2018.10.077
[32] W. Cai, Z. Zhang, Y. Jin, Y. Lv, L. Wang, K. Chen, and X. Zhou, Solar Energy, **188**, 441–449 (2019), https://doi.org/10.1016/j.solener.2019.05.081
[33] N.A. Bakr, A.K. Ali, S.M. Jassim, and K.I. Hasoon, ZANCO Journal of Pure and Applied Sciences, **29**(s4), s274-s280 (2017), https://doi.org/10.21271/ZJPAS.29.s4.31
[34] J.M.K.W. Kumari, N. Sanjeevadharshini, M.A.K.L. Dissanayake, G.K.R. Senadeera, and C.A. Thotawatthage, Ceylon Journal of Science, **45**(1), 33-41 (2016), http://dx.doi.org/10.4038/cjs.v45i1.7362
[35] D.L. Domtau, J. Simiyu, E.O. Ayieta, L.O. Nyakiti, B. Muthoka, and J.M. Mwabora, Surface Review and Letters, **24**(5), 1750065 (2017), https://doi.org/10.1142/S0218625X17500652
[36] Z.S. Wang, H. Kawauchi, T. Kashima, and H. Arakawa, Coordination Chemistry Reviews, **248**, 1381-1389 (2004), https://doi.org/10.1016/j.ccr.2004.03.006
[37] M.C. Kao, H.Z. Chen, S.L. Young, C.Y. Kung, and C.C. Lin, Thin Solid Films, **517**, 5096-5099 (2009), https://doi.org/10.1016/j.tsf.2009.03.102
[38] F. Behrouznejad, S. Shahbazi, N. Taghavinia, H.P. Wu, and E. W-G. Diau, Journal of Materials Chemistry A, **4**, 13488-13498 (2016), https://doi.org/10.1039/C6TA05938D

7,379 % ЕФЕКТИВНІСТЬ ПЕРЕТВОРЕННЯ ЕНЕРГІЇ ЧИСЛЕННО ЗМОДЕЛЬОВАНОГО ТВЕРДОГО СОНЯЧНОГО ЕЛЕМЕНТУ СЕНСИБІЛІЗОВАНОГО БАРВНИКОМ З ТІОЦІАНАТОМ МІДІ (I) У ЯКОСТІ ДІРКОВОГО ПРОВІДНИКА

Елі Данладі[a], Мухаммад Кашиф[b], Томас О. Даніель[c], Кристофер У. Ачем[d], Метью Альфа[e], Майкл Г'ян[f]
[a]Фізичний факультет, Федеральний університет наук про здоров'я, Отукпо, штат Бенуе, Нігерія
[b]Школа електричної автоматизації та інформаційної інженерії, Тяньцзінський університет, Тяньцзінь 300072, Китай
[c]Фізичний факультет, Федеральний університет Алекса Еквуме, Ндуфу Аліке, штат Ебоні, Нігерія
[d]Центр розвитку супутникових технологій NASRDA, Абуджа, Нігерія
[e]Фізичний факультет, Нігерійський армійський університет, Біу, штат Борно, Нігерія
[f]Фізичний факультет, Освітній університет, Віннеба, Гана

Предметом дослідження був пошук альтернативи рідкому електроліту в сонячних елементах, сенсибілізованих барвником (DSSC), щодо фотоелектричних властивостей. Тут шляхом моделювання ми повідомили про продуктивність сонячного елемента, сенсибілізованого барвником, замінивши рідкий електроліт на дірковий провідник з мідного (I) тіоціанатуэ(CuSCN). Дослідження проводилося за допомогою програмного забезпечення для моделювання сонячної ємності (SCAPS), яке базується на рівняннях Пуассона та безперервності. Моделювання проводилося на основі запропонованої n-i-p архітектури FTO/TiO2/N719/CuSCN/Pt. Результат початкового пристрою дав ефективність перетворення потужності (PCE) - 78,32 %, коефіцієнт заповнення (FF) - 5,71 %, щільність струму короткого замикання (Jsc) - 6,23 мАсм$^{-2}$, і напругу холостого ходу (Voc) - 1,17 В. Після оптимізації вхідних параметрів для отримання 1×109 см-2 для щільності дефектів інтерфейсу CuSCN/N719, 280 К для температури, 1,0 мкм для товщини барвника N719, 0,4 мкм для товщини TiO2, Pt для зворотного контакту металу та 0,2 мкм для товщини CuSCN , було отримано загальну продуктивність пристрою 7,379 % для PCE, 77,983 % для FF, 7,185 mAcm^{-2} для Jsc та 1,317 V для Voc. У порівнянні з початковим пристроєм, оптимізовані результати показали покращену продуктивність приблизно в 1,29 рази, 1,15 рази та 1,13 рази в PCE, Jsc і Voc порівняно з початковим пристроєм. Отримані результати є обнадійливими, і одержані дані можуть послужити базою для дослідників, які беруть участь у виготовленні нових високопродуктивних твердотільних DSSC, щоб зрозуміти їхню привабливість для масштабованості в галузі.

Ключові слова: ssDSSC, тіоціанат міді, дірковий провідник, SCAPs